ChemComm

Accepted Manuscript

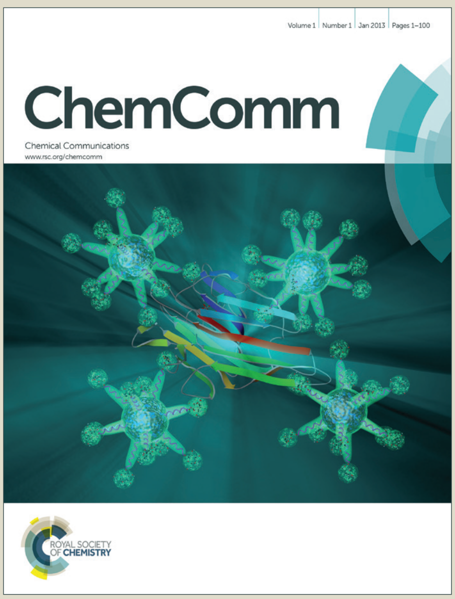

This is an *Accepted Manuscript*, which has been through the Royal Society of Chemistry peer review process and has been accepted for publication.

Accepted Manuscripts are published online shortly after acceptance, before technical editing, formatting and proof reading. Using this free service, authors can make their results available to the community, in citable form, before we publish the edited article. We will replace this *Accepted Manuscript* with the edited and formatted *Advance Article* as soon as it is available.

You can find more information about *Accepted Manuscripts* in the Information for Authors.

Please note that technical editing may introduce minor changes to the text and/or graphics, which may alter content. The journal's standard Terms & Conditions and the Ethical guidelines still apply. In no event shall the Royal Society of Chemistry be held responsible for any errors or omissions in this *Accepted Manuscript* or any consequences arising from the use of any information it contains.

ROYAL SOCIETY OF CHEMISTRY

www.rsc.org/chemcomm

Please do not adjust margins

Journal Name

COMMUNICATION

Thermally activated delayed fluorescence with circularly polarized luminescence characteristics†

Received 00th January 20xx,
Accepted 00th January 20xx

DOI: 10.1039/x0xx00000x

www.rsc.org/

Takuro Imagawa,‡[a] Shuzo Hirata,‡*[b] Kenro Totani,[a] Toshiyuki Watanabe[a] and Martin Vacha[b]

A metal-free aromatic compound with a chiral carbon sandwiched between a donor moiety and an acceptor moiety was designed. Under thermally activated delayed fluorescence, the compound displayed a photoluminescence quantum yield of 26%, and showed circularly polarized luminescence with a dissymmetry factor of 10^{-3}.

Metal-free aromatic molecules displaying thermally activated delayed fluorescence (TADF) are becoming important for future display and lighting applications.[1-3] When using TADF molecules as emitters in organic light-emitting diodes (OLEDs), electronically generated triplet excitons, which do not generally result in emission for metal-free aromatic emitters, can be extracted as a delayed fluorescence through reverse intersystem crossing (RISC) from the lowest triplet excited state (T_1) and the lowest singlet excited state (S_1). The efficient RISC process is facilitated by the small energy difference between S_1 and T_1, ΔE_{ST}, which is accomplished by leveraging steric hindrance in the molecule to induce a large separation between the highest occupied molecular orbital (HOMO) and the lowest unoccupied molecular orbital (LUMO).[4] Recent reported internal electroluminescence quantum yields using metal-free TADF molecules have reached nearly 100%.[1-3] Therefore, display and lighting applications using the TADF should be developed.

In flat panel displays using OLEDs, films composed of a polarizer and a quarter-wave plate are typically used to reduce reflectance from the surroundings for higher image contrast (See Fig. S1a, ESI†).[5] However, half of the emission from the OLEDs is then absorbed by the polarizer because there is no polarized emission from the emitting layer when conventional TADF molecules are used as emitters (Fig. S1b, ESI†). If TADF molecules with circularly polarized luminescence (CPL) could be developed, efficient electroluminescence from the TADF molecules can be extracted without absorption loss to the polarizer, leading to an energy savings in the OLED display (Fig. S1c, ESI†). While previous reports have detailed fluorescence compounds with CPL characteristics,[6,7] compounds with CPL as well as TADF characteristics have not been reported.

Here, we report a metal-free aromatic compound that displays both CPL and TADF characteristics. A metal-free aromatic molecule with a chiral carbon sandwiched between a triphenyl amine (TPA) moiety as a donor and naphthacen-5(12*H*)-one (NC) moiety as an acceptor was designed. Calculations using time-dependent density functional theory (TD-DFT) showed that the molecule's HOMO and LUMO are localized in the TPA and NC sections of the molecule at S_1, respectively. Because of the large spatial separation of the HOMO and LUMO, the molecule has a small ΔE_{ST} and shows green TADF with a photoluminescence quantum yield (Φ_{PL}) of 26% in host film. Enantiomers of the molecule showed circular dichroism (CD) and CPL, with dissymmetry factors of were $|1.2\times10^{-3}|$ and $|1.1\times10^{-3}|$ for CD and CPL, respectively. In addition, sign inversion between the CD and the CPL was observed for the molecule because of a large conformation change between the ground state (S_0) and the S_1.

The enantiomers of 12-(2-(diphenylamino)phenyl)-12-hydroxynaphthacen-5(12*H*)-one (DPHN) as shown in Fig. 1a were designed. Racemic DPHN was prepared by the nucleophilic addition reaction using n-BuLi as a catalyst (See Fig. S2, ESI†).[8] The enantiomers of DPHN were separated using a chiral column (Chiralpak ID, Daicel, Japan) (Fig. S3, ESI†). Ultraviolet (UV)-visible absorption and emission spectra were obtained using an UV-visible absorption spectrometer (V-560, Jasco, Japan) and a multi-channel analyzer (PMA-12, Hamamatsu, Japan), respectively. Emission lifetime was obtained using a fluorescence lifetime spectrometer (Quantaurus-Tau, Hamamatsu). Temperature dependence of the emission lifetime was measured using a cryostat (Optistat DN-V, Oxford, UK). Finally, CD and CPL were measured using a circular dichroism dispersion meter (J-720, Jasco) and spectrofluoropolarimeter (CPL-200, Jasco), respectively.

[a] Department of Organic and Polymer Materials Chemistry, Tokyo University of Agriculture and Technology, 2-24-16 Naka, Koganei, Tokyo 184-8588, Japan
[b] Department of Organic and Polymeric Materials, Tokyo Institute of Technology, 2-12-1, Ookayama, Meguro, Tokyo 152-8552, Japan.
[c] E-mail: hirata.s.af@m.titech.ac.jp
† Electronic supplementary information (ESI) available. See DOI: 10.1039/x0xx00000xj
‡ These authors contributed equally to the work.

ChemComm Accepted Manuscript

Please do not adjust margins

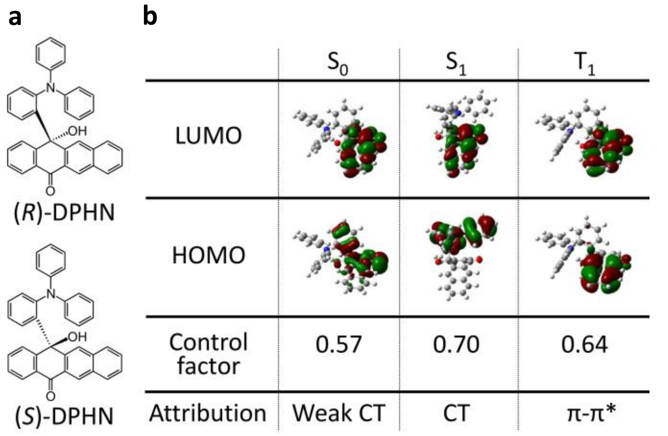

Fig. 1 (a) Chemical structures of (*R*)-DPHN and (*S*)-DPHN. (b) Molecular conformations and molecular orbitals of (*R*)-DPHN calculated using TD-DFT calculations at the B3LYP/6-31G(d,p) level. Molecular orbitals related to transitions with control factors larger than 0.3 are described. Other local minimum conformations at S_0, S_1, and T_1 are shown in Figs. S7, S9, and S10 of ESI†, respectively

Figure 1b shows a representation of the HOMOs and LUMOs of (*R*)-DPHN, as calculated using TD-DFT at the B3LYP/6-31G(d,p) level of theory, as implemented in Gaussian09.[9] For the optimized S_0 structure, the transition that generates the first absorption band has weak charge transfer (CT) character. For the optimized S_1, pure CT character between the HOMO and LUMO was observed. In the S_1 with pure CT character, the HOMO is localized over the TPA unit of (*R*)-DPHN while the LUMO is localized over the NC one. In contrast, π-π* character was mainly observed for the transition between S_0 and T_1. Because of the π-π* character of T_1, the energy of T_1 was slightly lower relative to the energy of S_1. Consequently, ΔE_{ST} did not become completely zero; indeed, ΔE_{ST} determined by the energy difference between the S_1 and T_1 was 0.07 eV. This ΔE_{ST} is significantly small compared with that of conventional fluorescent molecules, and, therefore, generation of TADF characteristics is anticipated for DPHN.

DPHN showed small ΔE_{ST} in solution. Figure 2a shows the absorption, fluorescence, and phosphorescence spectra of DPHN in toluene solution. DPHN has a first absorption band at around 400 nm as a shoulder of a large absorption peak at 363 nm. DPHN displays a broad fluorescence spectrum devoid of distinct vibrational structures that has maximum wavelength at 513 nm. The spectral shape suggests that the green fluorescence is caused by a CT transition.[10] CT fluorescence characteristics are reasonable because the HOMO and LUMO of the S_1 are largely separated, as shown in Fig. 1b. In contrast, the phosphorescence spectrum (Fig. 2a) has a distinct vibrational structure. This indicates that the T_1 of DPHN contains a π-π* character,[8] which is reasonable as the HOMO and LUMO overlap in the NC region of the molecule in the T_1, as shown in Fig. 1b. Consequently, ΔE_{ST} determined as the energy difference of the onset between the fluorescence and phosphorescence spectra was 0.26 eV. This value is small compared with that of conventional chiral aromatic compounds showing CPL characteristics (See Fig. S4, ESI†),[11] and the small ΔE_{ST} observed is

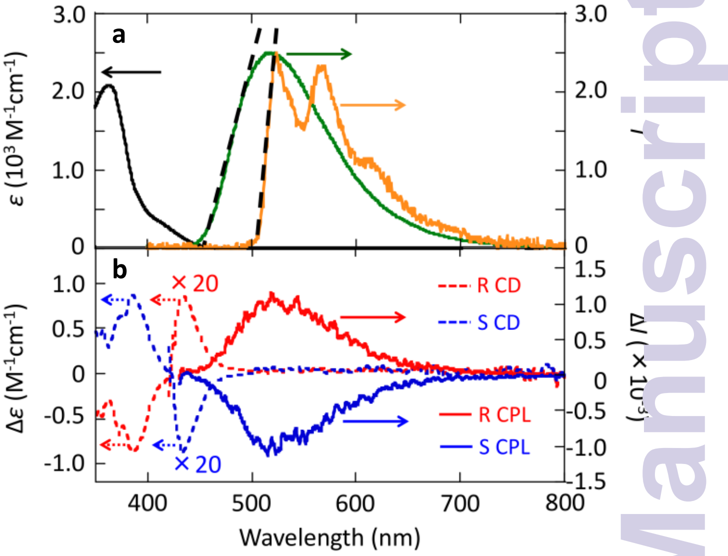

Fig. 2 Spectral characteristics of DPHN in toluene. (a) Absorption (black) and fluorescence (green) spectra at room temperature and phosphorescence spectrum (orange) at 77 K. Black dashed lines represent supporting lines to determine the S_1 and the T_1 energy. (b) CD and CPL spectra. Dotted and solid lines represent CD and CPL spectra, respectively. Blue and red represent data of (*R*)-DPHN and (*S*)-DPHN, respectively. Absorption and CD spectra were measured using solutions of DPHN in toluene (3.3×10^{-4} M). , Fluorescence, phosphorescence, and CPL spectra were measured using solutions of DHPN in toluene (8.8×10^{-5} M). For CD spectra at 420–500 nm, a DHPN concentration of 2.5×10^{-3} M was used to observe small CD peaks. For the CD spectra at 420–500 nm, the vertical scale was enlarged 20 times

consistent with the results of a TD-DFT calculation.

DPHN showed small oscillator strengths for absorption and fluorescence. Gaussian fitting to the shoulder absorption peak at around 400 nm suggested that DPHN has the longest absorption peak at 386 nm (See Fig. S5, ESI†). The molar absorption coefficient (ε) at 386 nm was 4.0×10^2 M^{-1} cm^{-1} (Fig. 2a). The value of the oscillator strength for absorption (F) at 386 nm is calculated using $F = 4.3\times10^{-9} n^{-1} \int \varepsilon d\nu$,[12] where n is the refractive index of toluene as a solvent and ν is the absorption wavenumber, and was evaluated to be 5.7×10^{-3}. This small F value is caused by the large HOMO and LUMO separation in the S_0, as shown in Fig. 1b.[3] The experimentally determined F is of comparable order to the F value computed with DFT shown in Table 1. Therefore, it is reasonable to presume that the conformation and molecular orbitals of DPHN optimized by DFT for the S_0 are useful to discuss other absorption characteristics such as CD. In addition, Φ_{PL} and the fluorescence lifetime (τ_f) of DPHN in toluene solution were 4% and 13.9 ns (See Fig. S6, ESI†), respectively. Here, we note that TADF does not typically appear in solutions exposed to air because solvated oxygen in the solvent quenches the triplet excitons of the TADF emitters,[13] resulting in single decay characteristics of the fluorescence lifetime from the TADF emitters. The fluorescence rate constant (k_f) calculated using $k_f=\Phi_{PL}/\tau_f$ from the values of Φ_{PL} and τ_f was 3.0×10^6 s^{-1}. The fluorescence oscillator strength (F') can be determined as 3.6×10^{-3} using the k_f value (See Section 4, ESI†).[14] This value is almost two orders of magnitude smaller than typical values of conventional

ChemComm Accepted Manuscript

This journal is © The Royal Society of Chemistry 20xx

Table 1 Photophysical characteristics of (*R*)-DPHN. TD-DFT at the B3LYP/6-31G(d,p) level is used for the calculations. Theoretical *F* and Δ*ε* are calculated for the optimized S_0 structure. The theoretical *F*′ is calculated for the optimized S_1 structure. Theoretical ΔE_{ST} is the energy difference between the S_1 energy in the optimized S_1 structure and the T_1 energy in the optimized T_1 structure. Data for other local minimum conformations at S_0 and S_1 are shown in Table S1 and S2 of ESI†, respectively. The experimental *F*′ value is determined by the method as described in Section 4 of the ESI. Experimental Δ*ε* is the value at 386 nm shown in Fig. 2b. Experimental ΔE_{ST} is the difference of the onset energy between the delayed fluorescence spectrum and the phosphorescence spectra as shown as dashed lines of Fig. 3a

Calculation				Experimental			
				Solution			Film
F (10^{-3})	F' (10^{-3})	$\Delta\varepsilon$ ($M^{-1}cm^{-1}$)	ΔE_{ST} (eV)	F (10^{-3})	F' (10^{-3})	$\Delta\varepsilon$ ($M^{-1}cm^{-1}$)	ΔE_{ST} (eV)
2.1	1.5	-0.42	0.07	5.7	3.6	-0.87	0.19

fluorescent molecules.[15] The *F*′ value computed using TD-DFT was of comparable order to the experimentally obtained value, as seen in Table 1. The small value of *F*′ is again caused by the large spatial separation between the HOMO and LUMO in the S_1, as shown in Fig. 1b.

The results of the DFT calculations suggested the appearances of CD and CPL for DPHN. As shown in Table 1, the difference in *ε* of the enantiomers of DPHN (Δ*ε*) was −0.42 M^{-1} cm^{-1} for the conformation of (*R*)-DPHN with the largest ratio at S_0 (Table S1, ESI†). In addition, the TD-DFT shows the appearance of Δ*ε* in the optimized S_1 structure (Table S2, ESI†), suggesting the appearance of CPL from (*R*)-DPHN. We deem the appearance of the CD and CPL to be caused by the chiral configuration between the HOMO and LUMO in the S_0 and S_1, respectively.

The enantiomers of DPHN display CD and CPL characteristics. Figure 2b shows the CD and CPL spectra of the DPHN enantiomers in toluene solution. The value of Δ*ε* for (*R*)-DPHN was −0.87 M^{-1} cm^{-1} at 386 nm. The experimentally observed value of Δ*ε* was comparable to that computed with DFT, shown in Table 1. Using the value of *ε* at 386 nm of 4.0×10^{2} M^{-1} cm^{-1}, the dissymmetry factor of CD (g_{abs}) can be estimated to be −1.2×10^{-3} from $g_{abs}=\Delta\varepsilon/\varepsilon$.[6] Although the experimentally observed absolute configuration of each enantiomer should be discussed, the single crystals of the enantiomers needed for X-ray characterization have not yet been obtained because of the large twisted structure of DPHN. Because the determination of absolute configurations of enantiomer pairs using DFT calculations has been reported in rigid aromatic structures,[16-19] we identified DPHNs showing the negative and the positive Cotton effect (CE) at 386 nm as (*R*)-DPHN and (*S*)-DPHN, respectively, according to the DFT results. In addition, (*R*)-DPHN and (*S*)-DPHN showed CPL at fluorescence wavelengths, as shown in Fig. 2b. The CPL dissymmetry factor (g_{lum}), defined as Δ*I*/*I*, where Δ*I* and *I* are the CPL and fluorescence intensities, respectively, was 1.1×10^{-3} for (*R*)-DPHN.[6] The value is moderate compared to other metal-free chiral aromatic compounds (Fig. S4, ESI†).[6,7]

More importantly, the CPL is opposite in sign to the CD at 386 nm in DPHN. As shown in Fig. 2b, (*R*)-DPHN and (*S*)-DPHN showed negative and positive CE for the CD at 386 nm while they had positive and negative CE for the CPL, respectively. The sign of CD and CPL is typically defined using the following equation,[20]

$$g_{LH} = 4\frac{|M_{LH}|}{|P_{HL}|}\cos\theta, \quad (1)$$

where g_{LH} is the dissymmetry factor that corresponds to g_{abs} for CD and g_{lum} for CPL, P_{HL} is the LUMO-to-HOMO electric transition dipole moment, M_{LH} is the HOMO-to-LUMO magnetic transition dipole moment, and *θ* is the angle between P_{LH} and M_{HL}. For the optimized S_0 structure, the negative value of g_{abs} can be explained from the negative value of cos*θ*, where *θ* =145° (Table S1, ESI†). However, the optimized S_1 conformation is different from the optimized S_0 conformation because of molecular relaxation after absorption. More specifically, the TPA and NC units are symmetric with respect to the chiral carbon in the S_0, but the NC unit position substantially changes when the molecule is excited to the S_1, as shown in Fig. 1b. The TPA location changes *θ* from 145° to [illegible] (Table S2, ESI†), causing the g_{LH} value to change from negative to positive. Such sign inversion between the CD signal for the [illegible] absorption band and CPL has been reported.[21-24] Careful investigation revealed that (*R*)-DPHN has a very small positive CD peak at 430 nm, as shown in Fig. 2b. The small CD peak is also caused by the transition from HOMO located over the TPA unit to the LUMO over the NC unit for a local minimum conformation at [illegible] (See Section 6, ESI†). Because the ratio of the local minimum conformation is smaller than that of the most populated conformation presented in S_0 of Fig. 1b and the local minimum conformation has small Δ*ε* (See Table S1, ESI†), the CD value at 430 nm is very small compared with that of the main peak of the optimized S_0 structure at 386 nm, as observed in Fig. 1b.

Furthermore, DPHN showed TADF when doped into a solid host.

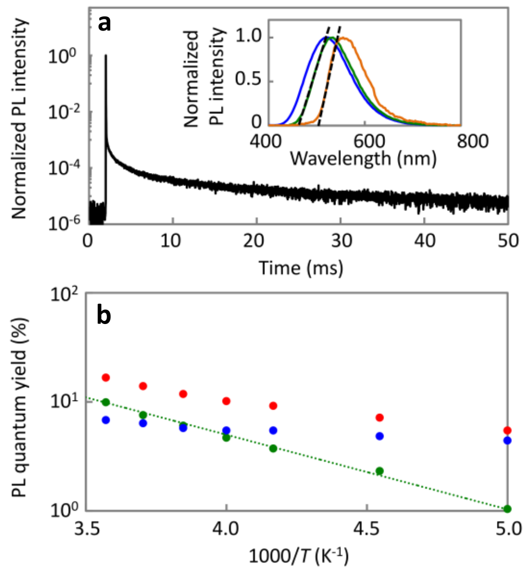

Fig. 3 Emission characteristics of 9 wt% DPHN-doped mCP film under excitation light at 340 nm. (a) Transient PL decay under vacuum conditions. The inset represents the PL spectra of prompt fluorescence at room temperature (blue; 0–300 ns), delayed fluorescence at room temperature (green; 0.7–50 ms), and phosphorescence component at 77 K (orange; 0.7–50 ms). Black dashed lines represent supporting lines to determine ΔE_{ST}. (b) Temperature dependence of Φ_{PF} (blue), Φ_{DF} (green), and Φ_{PL} (red)

ChemComm Accepted Manuscript

Figure 3a represents the fluorescence decay characteristics of 9 wt % DPHN-doped *N,N'*-4,4'-dicarbazole-3,5-benzene (mCP). Long delayed emission with the lifetime of milliseconds was observed, and this delayed emission was delayed fluorescence because the emission spectrum of the delayed component (green line in the inset of Fig. 3a) is similar to that of the prompt component (blue line in the inset of Fig. 3a). The orange line in the inset of Fig. 3a shows phosphorescence spectrum of the doped film, which was measured at 77 K. The energy difference of the onset between the delayed fluorescence spectrum and the phosphorescence spectrum was 0.19 eV.[10] This value is comparable to that computed with TD-DFT shown in Table 1. Therefore, it is supposed that the delayed fluorescence is caused by the TADF process through RISC between the T_1 and S_1.

Temperature-dependent delayed emission experiments revealed that the delayed emission is TADF. Figure 3b represents the temperature dependence of the prompt (Φ_{PF}) and delayed (Φ_{DF}) fluorescence quantum yields. Φ_{PF} and Φ_{DF} at room temperature were 11 and 15%, respectively, indicating that Φ_{PL} was 26%. Φ_{PF} was not dependent on temperature, while Φ_{DF} increased as the temperature increased (See Fig. S12, ESI†). The activation energy of Φ_{DF} was determined to be 0.14 eV. The lack of temperature dependence to Φ_{PF} in Fig. 3b indicates that internal conversion from the S_1 does not occur; instead, the small Φ_{PF} is caused by a large intersystem crossing (ISC) yield from the S_1 to the T_1. The small k_f value also leads to a large ISC yield, causing the small Φ_{PF}. For Φ_{DF}, the small Φ_{DF} is caused by not only the small k_f but also the moderate ΔE_{ST}. Although we note that DPHN has a small ΔE_{ST} compared to conventional fluorescent molecules with CPL characteristics, room temperature thermal energy is not sufficient to drive the RISC process from the T_1 to the S_1. Even with the few excitons that are thermally up-converted from T_1 to S_1, most of them return to T_1 before the generation of delayed fluorescence because the rate constant of the ISC is higher than the small k_f. Consequently, multiple cycles of ISC between the S_1 and the T_1 will occur without generating delayed fluorescence, resulting in a deactivation of the excitons from T_1.[3,4] Therefore, a decrease in ΔE_{ST} as well as an increase in k_f are necessary to obtain a large Φ_{DF}. For a large k_f, a large delocalization of the HOMO and LUMO, coupled with maintaining spatial separation of the HOMO and LUMO will be required.[3] The existence of the lowest triplet π-π* state, as shown in Fig. 1b, precludes the minimization of ΔE_{ST}. Therefore, molecules having pure lowest triplet CT states while keeping the chiral relationship of the HOMO and LUMO for the chiral carbon should be designed in the future.

In this article, we reported a metal-free aromatic compound with both CPL and TADF characteristics. The enantiomers of DPHN showed CD and CPL with a dissymmetry factor of 10^{-3} resulting from the chiral configuration between the HOMO and LUMO relative to a chiral carbon. Moreover, the CPL of the CT transition of DPHN possessed the opposite sign to the CD signal of the CT transition in the most populated conformation of DPHN because of a large configurational change of the HOMO and LUMO induced by large conformation change between the S_0 and S_1. In addition, DPHN showed TADF with Φ_{PL} of 26% in mCP film owing to a separation of the HOMO and LUMO. Arrhenius plots of the delayed fluorescence yield showed ΔE_{ST} of 0.14 eV. A further decrease of ΔE_{ST} is necessary to harvest triplet excitons as a delayed florescence. The molecular design of chiral aromatic compounds with the lowest triplet CT state will improve TADF yield while keeping CPL characteristics.

This research was supported by a Grant-in-Aid for Challenging Exploratory Research (24655175) and a Grant-in-Aid for Scientific Research on Innovative Areas "Photosynergetics" (26107014) from the Ministry of Education, Culture, Sports, Science and Technology, Japan.

Notes and references

1 H. Uoyama, K. Goushi, K. Shizu, H. Nomura and C. Adachi, *Nature*, 2012, **492**, 234-238.
2 Q. Zhang, B. Li, S. Huang, H. Nomura, H. Tanaka and C. Adachi, *Nat. Photon*., 2014, **8**, 326-332.
3 S. Hirata, K. Sakai, K. Masui, H. Tanaka, S. Y. Lee, H. Nomura, N. Nakamura, M. Yasumatsu, H. Nakanotani, Q. Zhang, K. Shizu, H. Miyazaki and C. Adachi *Nat. Mater*., 2015, **14**, 330-336.
4 A. Endo, K. Sato, K. Yoshimura, T. Kai, A. Kawada, H. Miyazaki and C. Adachi, *Appl. Phys. Lett*., 2011, **98**, 083302.
5 B. C. Kim, Y. J. Lim, J. H. Song, J. H. Lee, K.-U. Jeong, J. H. Lee, G.-D. Lee and S. H. Lee, *Opt. Express*, 2014, **22**, A1725-A1730.
6 J. E. Field, G. Muller, J. P. Riehl and D. Venkataraman, *J. Am. Chem. Soc*., 2003, **125**, 11808-11809.
7 H. Maeda, Y. Bando, K. Shimomura, I. Yamada, M. Naito, K. Nobusawa, H. Tsumatori and T. Kawai, *J. Am. Chem. Soc*., 2011, **133**, 9266-9269.
8 K. Nasu, T. Nakagawa, H. Nomura, C. -J. Lin, C. -H. Cheng, M. -R. Tseng, T. Yasuda and C. Adachi, *Chem. Commun*., 2013, **49**, 10385-10387.
9 M. J. Frisch *et al*, Gaussian 09, Revision D.01, Gaussian, Inc., Wallingford, CT, 2009.
10 Q. Zhang, J. Li, K. Shizu, S. Huang, S. Hirata, H. Miyazaki and C. Adachi, *J. Am. Chem. Soc*., 2012, **134**, 14706-14079.
11 C. Rosini, L. Franzini and P. Salvadori, *J. Org. Chem*., 1992, **57**, 6820-6824.
12 R. S. Mulliken, *J. Chem. Phys.*, 1939, **7**, 14-20.
13 G. Mehes, H. Nomura, Q. Zhang, T. Nakagawa and C. Adachi, *Angew. Chem. Int. Edit*., 2012, **51**, 11311-11315.
14 S. J. Strickler and R. A. Berg, *J. Chem. Phys.*, 1962, **37**, 814-822.
15 N. J. Turro, *Modern Molecular Photochemistry*, University Science Books, Sausalito, California, 1991.
16 N. Harada and K. Nakanishi, *Circular Dichroic Spectroscopy - Exciton Coupling in Organic Stereochemistry*, University Science Books, Mill Valley, CA, and Oxford University Press, Oxford, 1983.
17 N. Harada, K. Nakanishi and N. Berova, *Comprehensive Chiroptical Spectroscopy*, 2012, **2**, 115-166.
18 N. Harada and S. Kuwahara, *Comprehensive Chiroptical Spectroscopy*, 2012, **2**, 167-215.
19 N. Harada, Y. Takuma and H. Ueda, *J. Am. Chem. Soc*., 1976, **98**, 5408-5409.
20 F. S. Richardson, *Inorg. Chem*., 1980, **19**, 2806-2812.
21 T. Kimoto, T. Amako, N. Tajima, R. Kuroda, M. Fujiki and Y. Imai, *Asian J. Org. Chem*., 2013, **2**, 404-410.
22 G. Longhi, E. Castiglioni, S. Abbate, F. Lebon and D. A. Lightner, *Chirality*, 2013, **25**, 589-599.
23 S. Abbate, G. Longhi, F. Lebon, E. Castiglioni, S. Superchi, L. Pisani, F. Fontana, F. Torricelli, T. Caronna, C. Villani, R. Sabia, M. Tommasini, A. Lucotti, D. Mendola, A. Mele and D. A. Lightner, *J. Phys. Chem. C* 2014, **118**, 1682–1695.
24 T. Amako, K. Nakabayashi, T. Mori, Y. Inoue, M. Fujiki and Y. Imai, *Chem. Commun*., 2014, **50**, 12836-12839.

ChemComm Accepted Manuscript

This journal is © The Royal Society of Chemistry 20xx

Please do not adjust margins